

# Vibration based Structural Health Monitoring using output-only measurements under changing environment

A. Deraemaeker<sup>a</sup> E. Reynders<sup>b</sup> G. De Roeck<sup>b</sup> J. Kullaa<sup>c</sup>

<sup>a</sup> *ULB, Active Structures Laboratory*

*50 av Franklin Roosevelt, CP 165/42, B-1050 Brussels, Belgium*

<sup>b</sup> *K.U.Leuven, Department of Civil Engineering,*

*Kasteelpark Arenberg 40, B-3001, Heverlee, Belgium*

<sup>c</sup> *Helsinki Polytechnic Stadia, Department of Mechanical and Production  
Engineering*

*P.O. Box 4021, FIN-00099 City of Helsinki, Finland*

---

## Abstract

This paper deals with the problem of damage detection using output-only vibration measurements under changing environmental conditions. Two types of features are extracted from the measurements : eigen properties of the structure using an automated stochastic subspace identification procedure and peak indicators computed on the Fourier transform of modal filters. The effects of environment are treated

using factor analysis and damage is detected using statistical process control with the multivariate Shewhart-T control charts.

A numerical example of a bridge subject to environmental changes and damage is presented. The sensitivity of the damage detection procedure to noise on the measurements, environment and damage is studied. An estimation of the computational time needed to extract the different features is given, and a table is provided to summarize the advantages and drawbacks of each of the features studied.

*Key words:* Damage detection, Structural Health Monitoring, spatial filtering, modal filters, Environmental effects, output-only measurements, factor analysis, automatic stochastic subspace identification, statistical process control

---

## 1 Introduction

Structural Health Monitoring (SHM) problems have occupied many scientific communities for the last two decades. The problem is to be able to detect, locate and assess the extent of damage in a structure so that its remaining life can be known and possibly extended. As an alternative to the current local inspection methods, global vibration based methods have been widely developed over the years [1–4]. For the monitoring of bridges, actual and future trends in this domain are the use of vibration signals under ambient, unknown excitation due to wind or traffic (output-only data [5]), and the use of very large arrays of sensors (towards the concept of "smart dust" [6,7]). Full automation of the damage detection procedure is necessary for remote (i.e. web-based) monitoring applications.

---

*Email address:* [aderaema@ulb.ac.be](mailto:aderaema@ulb.ac.be) (A. Deraemaeker).

*URL:* <http://www.ulb.ac.be/scmero> (A. Deraemaeker).

The general methodology for detecting damage in structures is to extract meaningful features from the measured data. The features are monitored in order to detect changes due to damage. With the current trends of vibration based SHM, this problem is further complicated by the "output-only" nature of the data, the very large amount of information to be processed (due to the large sensor arrays), as well as the impact of environment which can cause changes in the monitored features of an order of magnitude equal or greater than the damage to be detected [8–11].

This paper aims at addressing these three issues. We will therefore focus on methods using output-only data. In order to overcome the problems linked to the very large amount of data, we propose to use spatial filtering techniques [12]. The main focus of this paper is on the effect and the removal of the environment. Two complementary approaches can be used for this purpose. The first one consists in extracting features which are strongly sensitive to damage but not very sensitive to the variability of the system and its environment. The second one consists in using a model of the impact of the environment on the features of interest in order to remove it from the extracted features. Emphasis is put on the possibility of full automation of the process.

Eigenfrequencies are classically used for damage detection. It is well known however that these features are often more sensitive to the environment than to the damage to be detected. On the other hand, mode shapes are less sensitive to the environment but the drawbacks are that the computational time is

high when large sensor arrays are used, and that the identification is not, up to now, fully automated. In order to overcome these problems, it was proposed in [13] to use the appearance of spurious peaks in the outputs of modal filters as feature for damage detection. It was shown that this feature is very sensitive to a local damage scenario, but not very sensitive to global changes due for example to environment. In addition, modal identification needs to be performed only at the beginning of the life of the structure, and the computation of the peak indicators is very fast and totally automatic. These advantages make it a very suitable alternative to modal identification techniques for damage detection.

In the second approach where one seeks to remove the effect of environment on the extracted features, three methods can be used. The first one consists in direct modelling of the impact of environment on the dynamical characteristics of a structure. This is a difficult task, because on one hand, there may be many factors which need to be taken into account, and on the other hand, the types of models (types of constitutive equations, parameters of these constitutive equations) to be used is generally unknown. One alternative is to identify models on the basis of measurements on a real structure. The models are aimed at representing accurately the relationship between measured dynamic features and measured environmental variables. They do not however have a real physical meaning (they only model an input-output relationship, so that the model and its parameters are not derived from physical laws). This restricts their use for the structure on which they have been identified. In practical applications, authors have limited their studies to the modelling of the relationship between the first eigenfrequencies and one environmental vari-

able (temperature). Examples of such are : the use of an AR (auto-regressive) model for the Z24 Bridge [10], the use of SVM (support vector machine) for the Ting Kau Bridge [14], or the use of a linear filter for the Alamosa Canyon bridge [15]. A major difficulty of the method is to determine where and which environmental factors to measure. In order to overcome this drawback, a last set of methods seeks to remove the variability due to environment without measuring the environmental factors. These methods rely on a decomposition of the covariance matrix of the features monitored over a long period of time with changing (but unmeasured) environmental conditions [16–19].

This paper is divided in four parts. The first part is dedicated to feature extraction using output-only measurements. Two methods are presented : the traditional approach which consists in extracting the eigen properties of the structure using stochastic subspace identification methods, and a novel approach which consists in computing peak indicators on the Fourier transform of the output of modal filters. For traditional operational modal analysis, a new process to automate the identification is presented. The second part deals with the modelling and removal of the environmental effects. A review of the different methods proposed in the literature which do not require to measure environmental variables is presented. The similarities between all these methods is stressed. The third part presents statistical process control as a tool for detecting deviation from the normal condition. The method consists in building univariate control charts with control limits which allow automatic and statistic treatment of the features for alarm triggering. In the last part, a numerical investigation using a finite element model of a three-span bridge subject to different environmental conditions is carried out. Two differ-

ent kinds of features are extracted automatically: eigen properties and peak indicators from modal filters. Factor analysis [16] is used for the removal of environmental effects. The different features are compared with respect to (i) their sensitivity to environment, (ii) their robustness to noise, (iii) the effect of factor analysis, (iv) the associated computational time. Finally, conclusions and perspectives are given.

## 2 Feature extraction based on output-only measurements

### 2.1 Output-only modal analysis

A first approach for feature extraction consists in identifying the eigenproperties of a structure using only the measured output signals. One of the fastest and most accurate methods is based on stochastic subspace identification [20,5]. The method identifies a discrete-time state-space model of the structure from output-only data. The only parameter in this model is the model order.

#### 2.1.1 Stochastic state-space model

The discrete state-space formulation of the dynamic equations of motion of a system sampled at constant time intervals  $k\Delta t$  is given by :

$$\begin{aligned} x_{k+1} &= A x_k + B u_k + w_k \\ y_k &= C x_k + D u_k + v_k \end{aligned} \tag{1}$$

where  $A$  is the discrete state matrix,  $x_k$  is the state vector at sample time  $k\Delta t$ ,  $B$  is the input matrix,  $u_k$  is the excitation force. Additional terms  $w_k$

and  $v_k$  represent the disturbances and measurement noise respectively.  $w_k$  and  $v_k$  have zero-mean and covariance matrices :

$$E \left[ \begin{pmatrix} w_p \\ v_p \end{pmatrix} \begin{pmatrix} w_q^T & v_q^T \end{pmatrix} \right] = \begin{pmatrix} Q & S \\ S^T & R \end{pmatrix} \delta_{pq} \quad (2)$$

The corresponding stochastic state-space formulation is defined as (1) without the deterministic input  $u_k$  :

$$\begin{aligned} x_{k+1} &= A x_k + w_k \\ y_k &= C x_k + v_k \end{aligned} \quad (3)$$

$x_k$  is assumed to be stationary with zero mean ( $E[x_k] = 0$ ) and covariance matrix  $\Sigma = E[x_k x_k^T]$ .  $w_k$  and  $v_k$  are independent of the actual state ( $E[x_k w_k^T] = 0$ ,  $E[x_k v_k^T] = 0$ ). For modal analysis, it is necessary to identify the matrices  $A$  and  $C$  only.

### 2.1.2 Stochastic Subspace identification and Operational Modal Analysis

The identification method presented in this paper is the reference-based data driven stochastic subspace method [5]. It is a generalization of the classical data-driven stochastic subspace method [20] in which the computation time is reduced, if necessary, by selecting only a few reference measurements for the so-called "past" measurements.

The main steps of the methods are given below in order to give to the reader a general idea of the computations needed to extract the modal properties. This will prove useful in section 5.4 where computational costs are discussed.

For more details on the theoretical aspects of the method, one should refer to [5].

- 1) Construction of the Hankel matrix : the output measurements are gathered in a block Hankel matrix with  $2i$  block rows and  $j$  columns. The first  $i$  block rows represent the past, whereas the next  $i$  block rows represent the future. For the future, all  $l$  sensors are retained (the number of rows is equal to  $li$ ) whereas for the past, only  $r$  reference sensors are taken into account (the number of rows is equal to  $ri$ ). It is only necessary to select references if the computation time is a problem (the gain in number of flops  $fl$  can be expressed as  $fl_{SSI/ref}/fl_{SSI} = ((l+r)/(2l))^2$  [21]) and/or if some channels are clearly more subject to noise than others. The Hankel matrix  $H$  reads :

$$H = \frac{1}{\sqrt{j}} \begin{pmatrix} y_0^{ref} & y_1^{ref} & \dots & y_{j-1}^{ref} \\ y_1^{ref} & y_2^{ref} & \dots & y_j^{ref} \\ \dots & \dots & \dots & \dots \\ y_{i-1}^{ref} & y_i^{ref} & \dots & y_{i+j-2}^{ref} \\ y_i & y_{i+1} & \dots & y_{i+j-1} \\ y_{i+1} & y_{i+2} & \dots & y_{i+j} \\ \dots & \dots & \dots & \dots \\ y_{2i-1} & y_{2i} & \dots & y_{2i+j-2} \end{pmatrix} = \begin{pmatrix} Y_p^{ref} \\ Y_f \end{pmatrix} \quad (4)$$

The size of the matrix is therefore  $(l+r)i \times j$  where  $j$  is a parameter chosen by the user. For statistical reasons, it is assumed that  $j \rightarrow \infty$ , so  $j$  should be rather large.



2) Perform an LQ factorization of  $H$  :

$$H = \begin{pmatrix} Y_p^{ref} \\ Y_f \end{pmatrix} = L Q^T \quad (5)$$

where  $Q \in \mathbb{R}^{(l+r)i \times j}$  is an orthonormal matrix ( $Q Q^T = I$ ) and  $L \in \mathbb{R}^{(l+r)i \times (l+r)i}$  is a lower triangular matrix. Note that the  $Q$  factor does not need to be calculated explicitly, which makes the subspace method computationally efficient since  $(l+r)i \ll j$ . The row indices of  $H$  are split in four parts : 1 corresponds to the  $r$  rows of the past, the first  $l$  rows of the future (corresponding to  $y_i \dots$ ) are split into  $r$  (2) and  $l-r$  (3) rows, and the following rows of the future correspond to 4. The LQ factorization therefore reads:

$$H = \begin{pmatrix} Y_p^{ref} \\ Y_f \end{pmatrix} = \begin{pmatrix} L_{11} & 0 & 0 & 0 \\ L_{21} & L_{22} & 0 & 0 \\ L_{31} & L_{32} & L_{33} & 0 \\ L_{41} & L_{42} & L_{43} & L_{44} \end{pmatrix} \begin{pmatrix} Q_1^T \\ Q_2^T \\ Q_3^T \\ Q_4^T \end{pmatrix} \quad (6)$$

3) Perform the following singular value decomposition:

$$\begin{pmatrix} L_{21} \\ L_{31} \\ L_{41} \end{pmatrix} = U S V^T \quad (7)$$

Choose the system order  $n$  and split the singular vectors and the singular

values in two parts:

$$USV^T = \begin{pmatrix} U_1 & U_2 \end{pmatrix} \begin{pmatrix} S_1 & 0 \\ 0 & S_2 \end{pmatrix} \begin{pmatrix} V_1 \\ V_2 \end{pmatrix} \quad (8)$$

in which  $S_1$  contains the first  $n$  singular values, and  $n$  is the chosen model order.

4) Compute the system matrices  $A$  and  $C$ :

$$O_i = U_1 S_1^{1/2} \quad (9)$$

$$\begin{pmatrix} A \\ C \end{pmatrix} = \begin{pmatrix} O_{i-1}^\dagger \begin{pmatrix} L_{41} & L_{42} & 0 \end{pmatrix} \\ \begin{pmatrix} L_{21} & L_{22} & 0 \\ L_{31} & L_{32} & L_{33} \end{pmatrix} \end{pmatrix} \begin{pmatrix} O_{i-1}^\dagger \begin{pmatrix} L_{21} & 0 & 0 \\ L_{31} & 0 & 0 \\ L_{41} & 0 & 0 \end{pmatrix} \end{pmatrix}^\dagger \quad (10)$$

$$= \mathcal{T}_i \mathcal{T}_r^\dagger$$

where  $\dagger$  denotes the Moore-Penrose pseudo-inverse of a matrix,  $O_i$  is the observability matrix and  $O_{i-1}$  is obtained by removing the last  $l$  rows of  $O_i$ .

5) Estimate  $Q$ ,  $R$  and  $S$  from equation (2) as:

$$\begin{pmatrix} Q & S \\ S^T & R \end{pmatrix} = \begin{pmatrix} \mathcal{T}_l - \begin{pmatrix} A \\ C \end{pmatrix} \mathcal{T}_r \end{pmatrix} \begin{pmatrix} \mathcal{T}_l - \begin{pmatrix} A \\ C \end{pmatrix} \mathcal{T}_r \end{pmatrix}^T \quad (11)$$

6) Using matrices  $A$  and  $C$ , the undamped eigenfrequencies  $f_{udi}$ , the damping ratios  $\xi_i$  and the mode shapes  $\phi_i$  of the structure can be calculated from

$$A = \Psi \Lambda \Psi^{-1}, \quad \Lambda = \text{diag}(\lambda_i) \in \mathbb{C}^{n \times n}, i = 1, \dots, n \quad (12)$$

$$\lambda_i^c = \frac{\ln \lambda_i}{\Delta t}, i = 1, \dots, n \quad (13)$$

$$f_{udi} = \frac{|\lambda_i^c|}{2\pi}, i = 1, \dots, n \quad (14)$$

$$\xi_i = \frac{\text{real}(\lambda_i^c)}{|\lambda_i^c|}, i = 1, \dots, n \quad (15)$$

$$\Phi = C\Psi, \quad \Phi = \begin{pmatrix} \phi_1 & \dots & \phi_n \end{pmatrix} \quad (16)$$

in which  $|\cdot|$  denotes the complex modulus.

### 2.1.3 Automatization of the Modal Analysis procedure

As the true system order is often unknown, it is a common practice in modal analysis to calculate the modal parameters for increasing model orders  $n$ . If  $n$  becomes higher than the true system order, also the noise is modeled, but if the noise is purely white, the mathematical poles that arise in this way are different for different model orders  $n$  which makes that they can be separated from the physical poles in a stabilization diagram, in which the eigenfrequencies corresponding to the identified poles are plotted for increasing model orders. Poles that arise due to the color of the noise can be separated from the physical poles based on physical criteria, like the value of the damping ratio or the shape of the mode. To clear out this diagram in order to only retain physical poles, only the poles of a certain model order for which the relative difference in eigenfrequency, damping ratio and MAC value with one of the poles of one lower model order is below a threshold value, are plotted. However, the stabilization diagram can still show some mathematical poles, especially for high model orders, which prevents the full automatization of the modal analysis procedure.

For this reason, recently a new criterion called *modal transfer norm* [22] has been introduced into the stabilization diagram which is a big step forward in the full automatization of modal analysis with subspace identification meth-

ods. For stochastic subspace identification, the modal transfer norm is based on the modal decomposition of the positive output power spectral density  $S_{yy}^+$ , which is defined as the Fourier transform of the positive lags of the cross-correlations between the measured outputs.  $S_{yy}^+$  can be calculated from [22]

$$S_{yy}^+(\omega) = C(zI - A)G + \frac{1}{2}\Lambda_0, \quad z = e^{j\omega\Delta t} \quad (17)$$

in which  $G$  and  $\Lambda_0$  can be calculated from

$$G = A\Sigma C^T + S \quad \Lambda_0 = C\Sigma C^T + R \quad \Sigma = A\Sigma A^T + Q \quad (18)$$

With a change of the state-space basis, the stochastic system description can be transformed into its modal form:

$$x_{k+1}^m = \Lambda x_k^m + w_k^m \quad (19)$$

$$y_k = C^m x_k^m + v_k \quad (19)$$

$$G^m = \Lambda \Sigma^m C^{mT} + S^m \quad (20)$$

in which  $x^m = \Psi^{-1}x$ ,  $w_k^m = \Psi^{-1}w_k$ ,  $C^m = C\Psi$ ,  $w_k^m$ ,  $\Sigma^m = \Psi^{-1}\Sigma\Psi^{-T}$  and  $S^m = \Psi^{-1}S$ . With this description, a modal model reduction of the stochastic system can be performed, resulting in the positive power spectral density of the reduced model which contains only mode  $i$  [22]:

$$S_{yy,i}^+(\omega) = c_i^m(z - \lambda_i)^{-1}g_i^m + \frac{\Lambda_{0i}}{2} \quad (21)$$

in which  $c_i^m$  is the  $i^{\text{th}}$  column of  $C^m$ ,  $g_i^m$  is the  $i^{\text{th}}$  row of  $G^m$  and  $\Lambda_{0i} = c_i^m \Sigma_{ii}^m c_i^{mT}$  with  $\Sigma_{ii}^m$  the  $i^{\text{th}}$  diagonal element of  $\Sigma^m$ . The quantity that is now introduced into the stabilization diagram is, for each mode [22]:

$$\|S_{yy,i}^+\|_\infty = \max_\omega \sigma(S_{yy,i}^+(\omega)) \quad (22)$$

where  $\sigma$  denotes the singular values of a matrix. The value of this modal transfer norm gives a measure of the error which is made when the  $i^{th}$  mode is removed from the full model. A stabilization diagram in which only the modes which have the highest modal transfer norms are plotted, is very clear [22].

This observation is now used for the automatization of operational modal analysis with the stochastic subspace identification method, which is highly desirable if the method is used for vibration monitoring. The new automatized method that is proposed in this paper consists of the following steps:

- 1) Determine an initial set of modal parameters using stochastic subspace identification and the stabilization diagram. This is the only step where user interaction is required.
- 2) For each new data set, perform a system identification for a certain model order  $n$ , which is sufficiently high so that the identified system certainly contains all physical poles of interest, and calculate the modal properties. Retain only the system poles that have realistic damping ratios. Sort the poles in decreasing order of modal transfer norm.
- 3) For each of the poles in the ordered new set, search for the pole in the previous set whose frequency is closest to this pole. Disregard this previous pole in next searches. If all previous poles are linked to a new pole, stop the search.
- 4) Repeat steps 2) and 3).

This automatized operational modal analysis procedure has been successfully validated on 20 series of 241 simulated bridge data sets, where in each set, the modal parameters change due to environmental effects and damage of the bridge, as is illustrated in section 5.3. For each data set, the method described

in this section succeeded in extracting the first 10 modes as desired. The model order  $n$  was set to 100 in each identification.

## 2.2 Features extracted from spatial filtering

A second approach for feature extraction is based on the concept of spatial filtering and peak indicators [23]. It is briefly summarized here below.

### 2.2.1 Spatial filtering and modal filters

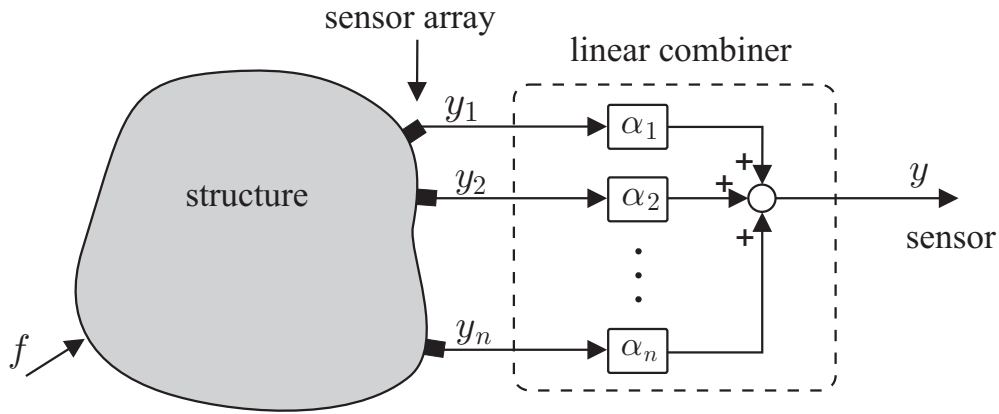


Fig. 1. Representation of the spatial filter using  $n$  discrete sensors and a linear combiner.

Let us consider a structure equipped with an array of  $n$  sensors (Fig.1). Spatial filtering consists in combining linearly the outputs of the network of sensors into one single output according to  $y = \sum \alpha_i y_i$ . Upon proper selection of  $\alpha_i$ , various meaningful outputs may be constructed, as, for example, modal filters. The idea behind modal filtering is to configure the linear combiner such that it is orthogonal to all  $N$  modes of a structure in a frequency band of interest except mode  $l$ . The modal filter is then said to be tuned to mode  $l$  and all the contributions from the other modes are removed from the signal. This

is illustrated in Fig. 2 where the square root of the power spectral density (PSD) of such a modal filter is represented, for a structure excited with a white noise spectrum. Because of spatial aliasing, there are some restrictions on the frequency band where modal filters can be built, for a given size of the sensor array.

### 2.2.2 Modal filtering with an array of sensors

The modal expansion of the FRF of the response on sensor  $k$  is given by :

$$Y_k(\omega) = \sum_{i=1}^N \frac{c_{ki}b_i}{(\omega_i^2 - \omega^2 + 2j\xi_i\omega_i\omega)} \quad (23)$$

where  $c_{ki}$  is the modal output gain of sensor  $k$  and  $b_i$  is the modal input gain.

If the  $n$  sensors in the array are connected to a linear combiner with gain  $\alpha_k$  for sensor  $k$  (Fig.1), the output of the linear combiner is  $y = \sum_{k=1}^n \alpha_k y_k$  and the global frequency response is :

$$G(\omega) = \sum_{k=1}^n \alpha_k Y_k(\omega) = \sum_{i=1}^N \frac{\{\sum_{k=1}^n \alpha_k c_{ki}\}b_i}{(\omega_i^2 - \omega^2 + 2j\xi_i\omega_i\omega)} \quad (24)$$

A modal filter which isolates mode  $l$  can be constructed by selecting the weighing coefficients  $\alpha_k$  of the linear combiner in such a way that

$$\sum_{k=1}^n \alpha_k c_{ki}(\omega) = \delta_{li} \quad (25)$$

Assume that the mode shapes of the system are identified using reference based stochastic subspace identification described in section 2.1.2. The identified mode shapes are gathered in the matrix of modal outputs  $\Phi$  (each column

corresponds to one modeshape projected on the sensors). Equation (25) is written in a matrix form :

$$\Phi^T \alpha = I \quad (26)$$

where  $\alpha$  is the matrix of modal filter coefficients (column  $l$  corresponds to  $\alpha_l$ ), and  $I$  is the identity matrix. The rank of  $\Phi^T$  is equal to the number of identified modes and it is assumed that there are more sensors than mode shapes.  $\Phi^T$  is therefore rank deficient. The inverse is computed using a singular value decomposition of  $\Phi^T$

$$\Phi^T = U S V^T \quad (27)$$

and truncating to the  $n$  highest singular values :

$$(\Phi^T)^+ = \sum_{i=1}^n \frac{1}{\sigma_i} v_i u_i^T \quad (28)$$

$(\Phi^T)^+$  is here the regularized pseudo-inverse of  $\Phi^T$ . Matrix  $\alpha$  is given by

$$\alpha = (\Phi^T)^+ I \quad (29)$$

For more details on the determination of the modal filter coefficients, the reader can refer to [24,25,12]. **Note that the coefficients of the modal filter are independent of the excitation type and location, and that the construction of modal filters in the case of modes closely spaced in frequency is not a problem, since the filtering is in the spatial domain.** In previous studies [13,23], the effect of damage on modal filters was studied. It was shown that a local damage produces spurious peaks in the frequency domain output of modal filters (Fig. 3a), whereas for global changes to



the structure (i.e. due to environment), the peak of the modal filter is shifted but the shape remains unchanged (Fig. 3b). **The appearance of peaks in the modal filters is due to the violation of the orthogonality condition between the initial modes of the structures used to compute the filters and the mode shapes of the structure in its present state.** Damage usually corresponds to a local stiffness change, whereas the environmental effects are usually more global and smooth, and mode shapes are much closer to the initial, undamaged ones. This explains why no spurious peaks (or only very low amplitude peaks) will appear and only the frequency of the filter will shift. It is clear however that if a global damage is considered, only very low amplitude peaks will appear, and if the environmental effect is very local, spurious peaks are likely to appear. This is of course a limitation of the method which can be overcome by using an ad-hoc treatment of the environmental effects as described in Section 3.

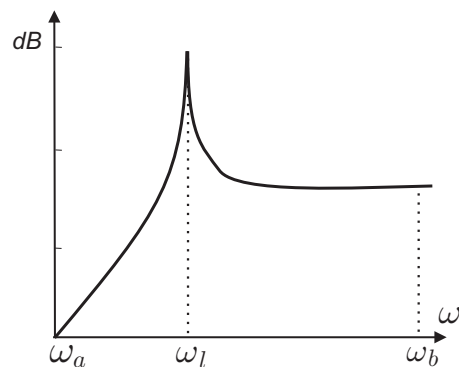


Fig. 2.  $\text{PSD}^{\frac{1}{2}}$  of the output of modal filter tuned to mode 1, the structure is excited with a white noise input spectrum

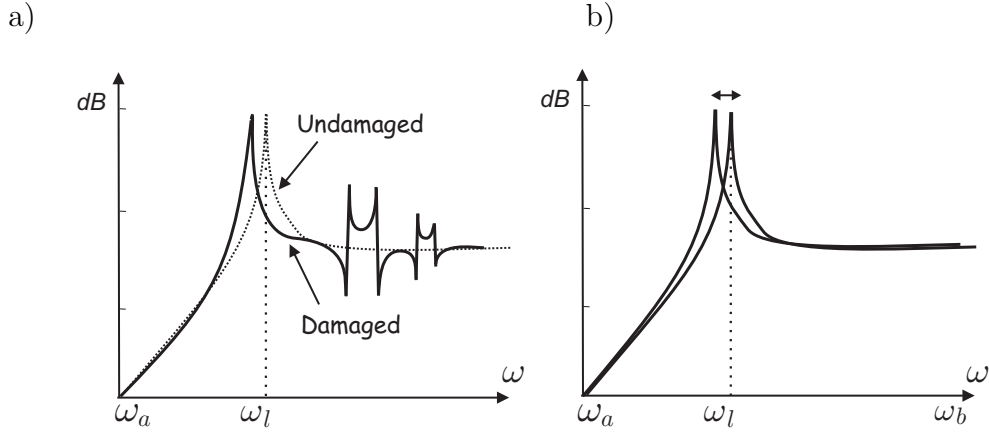
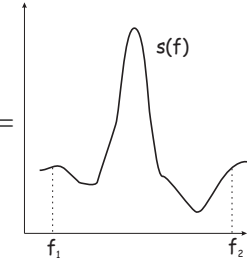


Fig. 3. Modal filter tuned to mode 1. a) Effect of damage, b) Effect of environment

### 2.2.3 Feature extraction

Each frequency point of the  $\text{PSD}^{\frac{1}{2}}$  of a modal filter can be used as a feature for damage detection. In practice however, this leads to a too large amount of features so that there is a need for data reduction. It is proposed to use a peak indicator, which reduces the amount of features to  $n_f \times n_e$  where  $n_f$  is the number of modal filters considered and  $n_e$  is the number of eigenfrequencies in the frequency bandwidth of the modal filter. The computation of this indicator follows the method presented in [26], where a discrete formulation is proposed. Here we use different notations and a continuous formulation. The entire frequency bandwidth is divided in frequency bands  $[f_1, f_2]$  around each natural frequency of the structure (the bandwidth is given in % of the natural frequency, typical values are 10 or 20 %). The following mean and variances are computed :

- The frequency center (FC) =  $\frac{\int_{f_1}^{f_2} f s(f) df}{\int_{f_1}^{f_2} s(f) df}$
  - The root variance frequency (RVF) =  $\left[ \frac{\int_{f_1}^{f_2} (f - FC)^2 s(f) df}{\int_{f_1}^{f_2} s(f) df} \right]^{\frac{1}{2}}$
- 

The peak indicator is given by :

$$I_{peak} = \frac{RVF\sqrt{3}}{FC(f_2 - f_1)} \quad (30)$$

It has the following properties :

- if  $s(f)$  is a Dirac function,  $I_{peak} = 0$
- if  $s(f) = Cst$ ,  $I_{peak} = 1$
- A drop in  $I_{peak}$  corresponds to the appearance of a peak.

#### 2.2.4 Pre-processing of the modal filters for feature extraction

In order for the peak indicator to be more sensitive (increase of signal-to-noise ratio), we use a technique called "second derivative matched filtering" [27].

Let  $x(\omega)$  be the signal to be filtered and  $f(\Omega)$  be the filtering function. The filtered signal is given by :

$$y(\omega) = \int_{-\infty}^{\infty} f(\Omega)x(\omega + \Omega)d\Omega \quad (31)$$

In order to remove background noise, the second derivative is computed :

$$y''(\omega) = \int_{-\infty}^{\infty} f(\Omega)x''(\omega + \Omega)d\Omega = \int_{-\infty}^{\infty} f''(\Omega - \omega)x(\Omega)d\Omega \quad (32)$$

This last expression shows that it is only necessary to derive the filtering function, which is much less sensitive to the noise than deriving the signal

itself. On the other hand, the filtering function needs to be twice differentiable. Although the philosophy of matched filtering is to have a filtering function equal to the equation of the peak to be detected, this choice is not adopted here (due to the complicated expression of the second derivative). Instead, a simpler and typical choice for such a function is a Gaussian distribution. There is in fact an analogy of this method with wavelet analysis where the so-called "mexican-hat" corresponds to the second derivative of the Gaussian [28]. The scaling factor in wavelet analysis is analog to the standard deviation of the Gaussian. An optimal choice of this factor allows to remove efficiently the noise in the initial signal. One example of second derivative matched filtering is given in Fig. 4. The filtered signal has a flat spectrum due to the second derivative and the peaks are enhanced by the filtering which makes  $I_{peak}$  more sensitive.

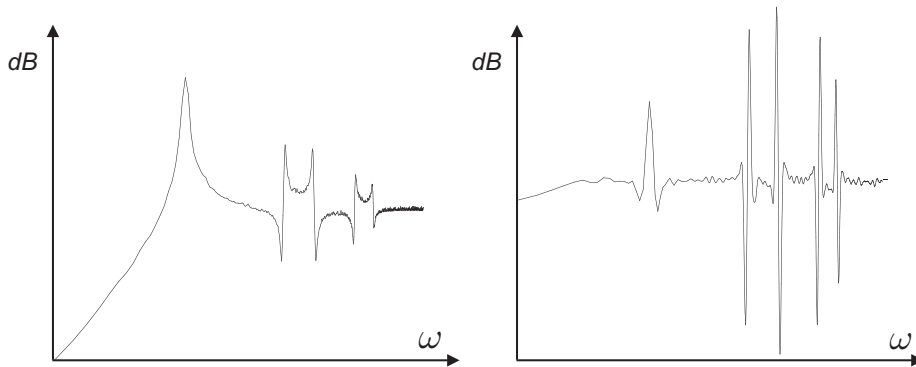


Fig. 4. Effect of Gaussian second derivative filtering using a "mexican hat" function  
 :

a) Original signal, b) Filtered signal

### 2.2.5 Further processing of features

In order to perform damage detection, features sensitive to damage should be selected. In the example of Fig. 3, one sees that the peak indicator for peak number 1 is not sensitive to damage since the peak is already present in the

undamaged filter. Therefore the number of features retained for damage detection is  $n_f \times (n_e - 1)$ . In the case where two peaks are very close in frequency, the frequency bands corresponding to these natural frequencies are merged, which reduces the number of features without affecting the efficiency of the peak detection (the peak indicator will be sensitive to the appearance of one, or the other, or both peaks).

There are two main advantages to this approach : (i) the number of sensors can be greatly reduced due to the spatial filtering, which reduces the amount of data, (ii) the feature extraction is very fast and fully automatic. It is therefore particularly well suited for remote web-based damage detection.

**Note that in the case where the input excitation is not white noise, extra peaks can appear in the PSD of the modal filters due to the color of noise. This is however not a problem if, in the identification process, these peaks have not been identified (which, as stated in Section 2.1.3 can be done easily based on physical criteria). Indeed, the peak indicators are computed only in frequency bands around the identified natural frequencies. This may therefore cause a false alarm only in the case where the peaks coming from the color of noise are close in frequency with the system poles.**

### 3 Modelling and removal of environmental effects

Many structures are subject to varying environmental conditions which affect their dynamical behavior. Examples are bridges subject to outdoors environmental variables such as temperature and humidity. Due to the difficulty of accurately modeling the impact of environment on the features extracted, it is desirable to be able to remove this impact without measuring environmental variables. The key idea is to identify a linear subspace in which the environmental effects lie. Projecting the features in the subspace orthogonal to the linear subspace identified allows to get rid of the environmental effects. This is explained in more details in the next section.

#### 3.1 General model of the environment

Let us assume that all the features are arranged in a vector  $x$ , one can write :

$$x = f(T, h, \dots) + g(\eta) \quad (33)$$

where  $\eta$  is the vector of variables independent of the environment (i.e. structural changes, damage, noise, ...), and  $(T, h, \dots)$  are the environmental variables (i.e. Temperature, humidity, ...). As mentioned earlier, function  $f$  is very difficult to identify, the general form being dependent on the structure considered and the type of features extracted. This general mapping function  $f$  can be decomposed into two different mappings as shown on Figure 5. The environmental factors  $(T, h, \dots)$  are transformed into a vector of *unobservable factors*  $\xi$ , by means of a non-linear mapping  $\mathcal{M}$  :

$$f(T, h, \dots) = \Lambda(\mathcal{M}(T, h, \dots)) \quad (34)$$

The terminology *unobservable factors* is borrowed from factor analysis [16]. This non-linear mapping is generally unknown and there is no need to identify it. The *unobservable factors*  $\xi$  are assumed to be statistically independent variables. A linear mapping  $\Lambda$  is used between the *unobservable factors* and the features (Fig 6). Equation (33) becomes :

$$x = \Lambda\xi + g(\eta) \quad (35)$$

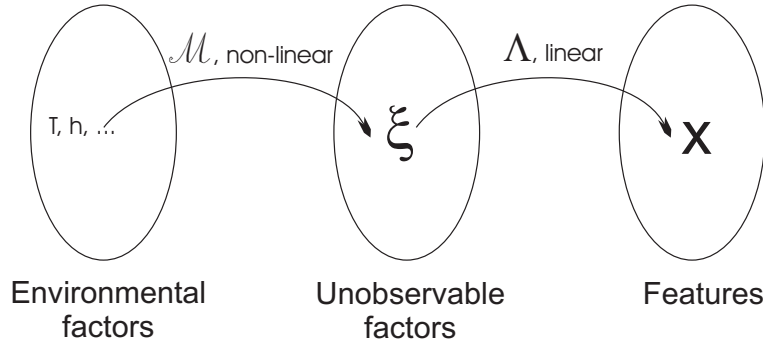


Fig. 5. Function  $f$  relating the dynamical features with the environmental variables is decomposed into a non-linear mapping  $\mathcal{M}$  and a linear mapping  $\Lambda$ , introducing statistically independent *unobservable factors*  $\xi$

If the number of *unobservable factors* is equal to the number of features, the new mapping is identical to function  $f$ ,  $\Lambda$  can be seen as an orthogonalization of the feature vector  $x$ . In this case  $g(\eta) = 0$  and the environment cannot be distinguished from the other variables in  $\eta$ . In order to remove the effects of environment on features and keep information about damage or structural changes, the dimension of  $\xi$  needs to be smaller than the number of features. One important parameter in the method is therefore the number of *unobservable factors*. This is discussed in the following section.

### 3.2 Model identification

In order to identify the linear mapping  $\Lambda$  between the *unobservable factors* and the features, it is necessary to measure the feature vector under changing environmental conditions, while the influence of other factors ( $\eta$ ) is small :

$$\varepsilon = g(\eta) \ll \Lambda\xi \quad (36)$$

This requires to extract features from the undamaged structure during a period of time in which all of the environmental effects to be removed manifest themselves (i.e. : monitoring a bridge after construction during a one year period of time).

Based on these measured features, two different approaches are presented, covariance based and data based techniques.

#### 3.2.1 Covariance based model identification

Assume that the feature vector  $x$  is sampled during a certain period of time. The covariance matrix of the features is given by :

$$\Sigma_x = E[xx^T] = E[(\Lambda\xi + \varepsilon)(\Lambda\xi + \varepsilon)^T] \quad (37)$$

where  $E$  is the mathematical expectation over the whole sampling time. *Unobservable factors* are supposed to have zero-mean and covariance matrix equal to identity. Equation (37) therefore reduces to :

$$\Sigma_x = \Lambda\Lambda^T + \Psi \quad (38)$$



where  $\Psi$  is the covariance matrix of  $\varepsilon$ . The problem is to be able to split the covariance matrix of measured features into the contribution of environment and the residual part. This is possible because of the assumption that  $\varepsilon \ll \Lambda\xi$ . Using singular value decomposition (SVD) of  $\Sigma_x$ , one gets :

$$\Sigma_x = USU^T \quad (39)$$

with

$$U^T U = I, S = \begin{bmatrix} S_1 & 0 \\ 0 & S_2 \end{bmatrix} \quad (40)$$

The left and right vectors are identical because  $\Sigma_x$  is a symmetric matrix, this is therefore equivalent to finding the eigenvalues and eigenvectors of  $\Sigma_x$ .

Matrix  $S$  is split in two parts :  $S_1 = \text{diag}(\sigma_1^2, \sigma_2^2 \dots \sigma_m^2)$  is a diagonal matrix with the square of the first  $m$  singular values on the diagonal, ranked by decreasing order, and  $S_2 = \text{diag}(\sigma_{m+1}^2 \dots \sigma_n^2)$ , where  $n$  is the size of the feature vector  $x$ . The splitting (value of  $m$ ) can be done in two ways:

- Plotting the singular values ranked in decreasing order, a drop in the singular values occurs :  $m$  is chosen as the value before this drop. This is equivalent to finding the rank of  $\Sigma_x$ , i.e. the size of the subspace of  $\Sigma_x$ .

**In practice, however, this drop rarely occurs clearly, which is the motivation for the second method of splitting:**

- Define the indicator :

$$I = \frac{\sum_{i=1}^m \sigma_i^2}{\sum_{i=1}^n \sigma_i^2} \quad (41)$$

and determine  $m$  as the lowest integer such that  $I > e(\%)$ , where  $e$  is a threshold valued (i.e. 95 %) The meaning of this threshold is as follows :  $m$  *unobservable factors* are needed in order to explain  $e\%$  of the variance in the observed data.

Matrix  $U$  is also split in two parts :

$$U = [U_1 U_2] \tag{42}$$

and this splitting allows to identify  $\Lambda$  and  $\Psi$  :

$$\Lambda = U_1 \sqrt{S_1} \tag{43}$$

$$\Psi = U_2 S_2 U_2^T \tag{44}$$

This method is often referred to as Principal Component Analysis (PCA, [17,29,18]), the vectors of  $U_1$  are called principal components. In factor analysis, the column vectors of  $\Lambda$  are called factor loadings. Each column of the factor loading matrix is equal to a principal component multiplied by the square root of the corresponding singular value. A slight difference with the method of PCA, lies in the fact that  $\varepsilon$  are called *unique factors* and are assumed to be uncorrelated, which means that  $\Psi$  is diagonal. In order to achieve this, an iterative process is needed in which the first iteration corresponds to the PCA described here above. Further iterations allow to converge to a diagonal matrix  $\Psi$  [30]. Practical applications show however that the resulting linear subspace  $\Lambda$  only slightly changes during the iterations. Moreover, the validity of the hypothesis of a diagonal  $\Psi$  matrix is somehow doubtful in many applications in which the processing needed to extract the features results in a non-diagonal covariance matrix for  $\varepsilon$ .

### 3.2.2 Data based model identification

An alternative to covariance based methods is to perform the SVD directly on the sampled feature vector :

$$x = U\sqrt{S}V^T \quad (45)$$

It can easily be shown that the matrices  $U$  and  $S$  are identical to the ones found when performing the  $SVD$  on  $\Sigma_x$ . One drawback of the method is that the  $SVD$  is performed on a large rectangular matrix, which makes it computationally less attractive (note that in applications where matrix  $V$  is of interest, the situation is different). Selecting the size of the linear subspace can be done in the same way as for the covariance based method. Note however that the interpretation of the threshold as the representation of a given percentage of the covariance matrix is not straightforward and usually not given when data based  $SVD$  is performed (see i.e. [19]).

### 3.3 Removal of environmental effects

In the previous section, we have discussed the identification of the linear operator  $\Lambda$ . In order to remove the part of the features which belongs to the linear subspace from the measured features, we need to solve the following estimation problem : find  $\tilde{\xi}$  which minimizes :

$$\|x - \Lambda\tilde{\xi}\|^2 \quad (46)$$

The choice of the norm  $\|\cdot\|^2$  leads to different well known estimators : using an  $L_2$  (euclidian) norm leads to the classical least-square estimator, which is the Moore-Penrose pseudo-inverse of  $\Lambda$ :

$$\tilde{\xi} = (\Lambda^T \Lambda)^{-1} \Lambda^T x \quad (47)$$

Because of the properties of the *SVD* ( $U_1^T U_1 = Id$ ), this expression reduces to :

$$\tilde{\xi} = S_1 U_1^T x \quad (48)$$

If the subspace of principal components  $U_1$  is used instad of  $\Lambda$ , the estimated value of  $\tilde{\xi}$  is given by :

$$\tilde{\xi} = (U_1^T U_1)^{-1} U_1^T x \quad (49)$$

which reduces to :

$$\tilde{\xi} = U_1^T x \quad (50)$$

This approach is the most widely used [17–19].

Two alternatives which come from statistical analysis are presented in [31]. The first one is derived using a maximum likelihood approach (Bartlett's factor score) :

$$\tilde{\xi} = (\Lambda^T \Psi^{-1} \Lambda)^{-1} \Lambda^T \Psi^{-1} x \quad (51)$$

and the second one is derived using a Bayesian approach (Thomson's factor score) :

$$\tilde{\xi} = (I + \Lambda^T \Psi^{-1} \Lambda)^{-1} \Lambda^T \Psi^{-1} x \quad (52)$$

Bartlett's factor score is unbiased whereas Thomson's factor score is biased. The average prediction error of Thomson's factor score is however lower. The last two estimators take into account the covariance matrix of  $\varepsilon$ . This can prove useful if different types of features affected by different levels of noise are used (i.e. it is well known that extracted mode shapes are much more noisy than eigenfrequencies). The estimation will put less weight on the more uncertain parameters (large terms on the diagonal of  $\Psi$ ), which will result in a better estimation, taking into account the uncertainties on the different features. This approach is well known in statistical estimation theory [32] but of rather limited application because matrix  $\Psi$  is generally not known. Here however, matrix  $\Psi$  is given by the identification, so that the approach can be used. It should be noted however that there may be problems in computing the inverse of  $\Psi$  if the classical PCA is used. In fact, if the iterative method of factor analysis is used, matrix  $\Psi$  is diagonal which makes it invertible. On the other hand, matrix  $\Psi$  resulting from a first iteration of the PCA is not of order  $n$ , so that it cannot be inverted. One way to work around this problem is to keep only the diagonal terms in  $\Psi$ . In this manner, the simplified matrix is invertible, and one keeps the weighting between the uncertainties related to the different features in the estimation. This is also motivated by the fact that the iterations do not modify the subspace  $\Lambda$  by a large extent as stated in section 3.2.1, so that the  $\Psi$  matrix can be approximated with a good accuracy by keeping only the diagonal terms.

Using one of the estimators defined above, we can now compute the residual, which is the part of the features orthogonal to the linear subspace spanned by  $\Lambda$  :

$$\varepsilon = x - \Lambda \tilde{\xi} \quad (53)$$

The new feature vector is given by  $\varepsilon$ , it corresponds to the dynamic features from which the environmental effects have been removed.

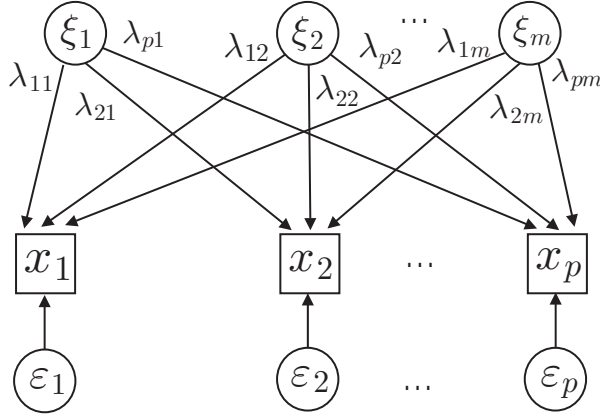


Fig. 6. Orthogonal factor model.

#### 4 Statistical Process Control

Control charts [33] are used here for damage detection. They are a tool of statistical quality control to detect if the process is out of control. It plots the quality characteristic as a function of the sample number. The chart has lower and upper control limits, which are computed from those samples only when the process is assumed to be in control. When unusual sources of variability are present, sample statistics will plot outside the control limits. In that occasion an alarm is triggered. There exist different control charts, differing on

their plotted statistics. Several univariate and multivariate control charts for damage detection were studied in [34].

In this paper the features for damage detection are the largest principal components of all of the unique factors. The number of principal components was determined using the criterion that they explained at least 99.9% of the variation in the features of all samples.

Principal component analysis, PCA is a linear transformation that transforms the data to a new coordinate system such that the greatest variance by any projection of the data comes to lie on the first coordinate (called the first principal component), the second greatest variance on the second coordinate, and so on. PCA can be used for dimensionality reduction in a dataset while retaining those characteristics of the dataset that contribute most to its variance, by keeping the first principal components and ignoring the remaining ones.

It can be shown that principal component analysis reduces to finding the eigenstructure of the data covariance matrix. Alternatively, PCA can be done by finding the singular value decomposition (SVD) of the data matrix or a spectral decomposition of the data covariance matrix. [30]. The first principal component is the eigenvector corresponding to the largest eigenvalue of the covariance matrix, The second principal component is the eigenvector corresponding to the second largest eigenvalue, and so on. In the following, the spectral decomposition of the covariance matrix is only presented.

Let  $\mathbf{X}$  be an  $n \times p$  data matrix. Since the data covariance matrix  $\Sigma_{\mathbf{X}}$  ( $p \times p$ ) is symmetric, its spectral decomposition can be written as

$$\Sigma_{\mathbf{X}} = E(\mathbf{X}^T \mathbf{X}) = \mathbf{P} \Lambda \mathbf{P}^T \quad (54)$$

where  $\Lambda$  is a diagonal matrix whose elements are the eigenvalues of the symmetric covariance matrix  $\Sigma_{\mathbf{X}}$ .  $\mathbf{P}$  is a  $p \times p$  orthogonal matrix ( $\mathbf{P} \mathbf{P}^T = \mathbf{P}^T \mathbf{P} = \mathbf{I}$ ) whose  $j$ th column is the eigenvector corresponding to the  $j$ th eigenvalue.

The scores  $\mathbf{Y}$  are the new values expressed in the principal component base and are computed by

$$\mathbf{Y} = \mathbf{X} \mathbf{P} \quad (55)$$

and the covariance matrix of  $\mathbf{Y}$  is

$$\Sigma_{\mathbf{Y}} = E(\mathbf{Y}^T \mathbf{Y}) = E[(\mathbf{X} \mathbf{P})^T (\mathbf{X} \mathbf{P})] = E(\mathbf{P}^T \mathbf{X}^T \mathbf{X} \mathbf{P}) = \mathbf{P}^T \Sigma_{\mathbf{X}} \mathbf{P} \quad (56)$$

Substituting Equation (54) we get

$$\Sigma_{\mathbf{Y}} = \mathbf{P}^T \mathbf{P} \Lambda \mathbf{P}^T \mathbf{P} = \Lambda \quad (57)$$

The new variables are therefore uncorrelated and have a variance equal to the corresponding eigenvalue. In the dimensionality reduction, only the first eigenvectors (first columns of  $\mathbf{P}$ ) are used to compute the new variables.



The multivariate control chart used in this study is the Shewhart  $T$  control chart [33], where the plotted characteristic is:

$$T^2 = n(\bar{\mathbf{x}} - \bar{\bar{\mathbf{x}}})^T \mathbf{S}^{-1}(\bar{\mathbf{x}} - \bar{\bar{\mathbf{x}}}) \quad (58)$$

where  $\bar{\mathbf{x}}$  is the subgroup average,  $\bar{\bar{\mathbf{x}}}$  is the process average, which is the mean of the subgroup averages when the process is in control, and  $\mathbf{S}$  is the matrix consisting of the grand average of the subgroup variances and covariances.

The upper control limit is

$$\text{UCL} = \frac{p(m+1)(n-1)}{mn-m-p+1} F_{\gamma, p, mn-m-p+1} \quad (59)$$

where  $p$  is the dimension of the variable,  $n$  is the subgroup size,  $m$  is the number of subgroups when the process is assumed to be in control, and  $F_{\gamma, p, mn-m-p+1}$  denotes the  $\gamma$  percentage point of the  $F$  distribution with  $p$  and  $mn-m-p+1$  degrees of freedom. The  $F$  distribution is used because in factor analysis  $x$  is assumed to be Gaussian.

## 5 Numerical example

### 5.1 Presentation of the structure

The structure considered is a three-span bridge similar to the one presented in [18,23] (Fig 7). The motion is restricted to in plane vibrations. It is made of two materials : steel and concrete. The Young's modulus of these materials is assumed to be temperature dependant (Fig 8). During the monitoring, the structure is subject to gradients of temperature. The reference temperature

(right hand side) varies from  $-15$  to  $+45$  °C, whereas it varies from  $-15$  to  $0$  °C on the left hand side (a linear interpolation is assumed between the left and right end temperatures). The system is excited by a uniform pressure acting on the first span of the bridge (see Fig 7). The pressure is assumed to be a band limited white noise excitation (0-100 Hz, containing the first 10 mode shapes of the structure).

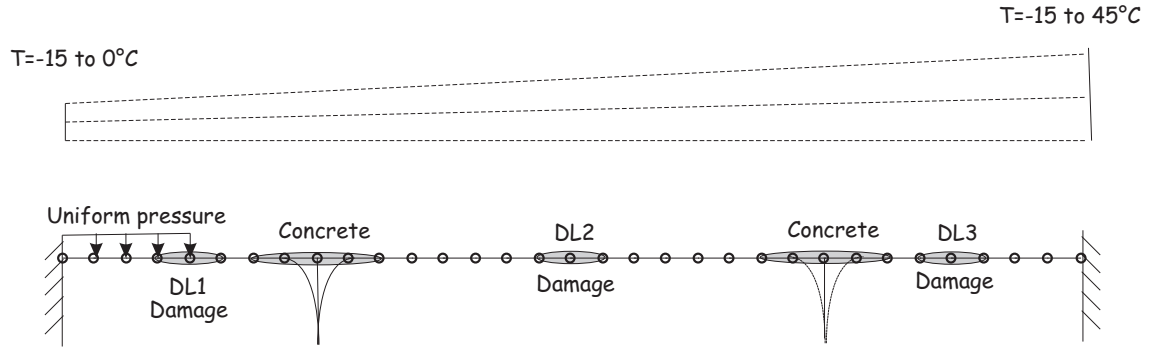


Fig. 7. Three-span bridge subject to different temperature gradients and damage

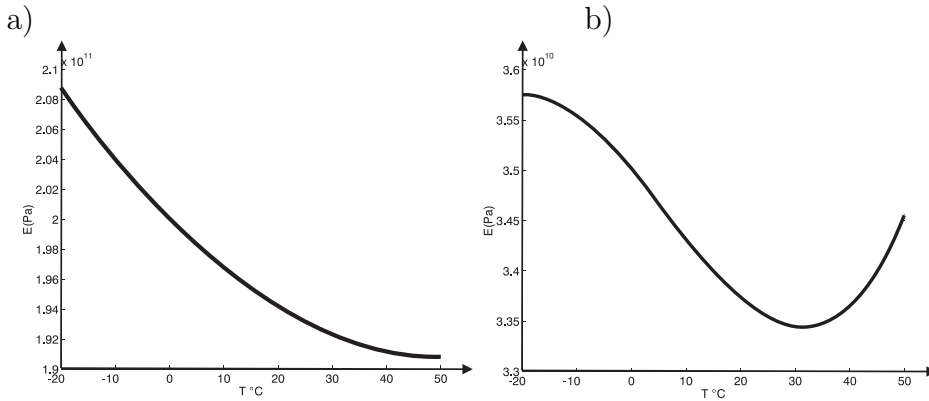


Fig. 8. Temperature dependence for the Young's Modulus of the two materials :

a) Steel, b) Concrete

## 5.2 Computation of the response of the bridge

The bridge is discretized with 32 Euler Bernoulli finite elements using the Structural Dynamics Toolbox (SDT [35]) under Matlab. The response is com-

puted in the time domain using an in-house time integration scheme based on the Duhamel's formula [36] . A total of 29 accelerometers are placed, one at each node of the finite element model (except boundary conditions). The time domain response (100s at a sampling rate of 1000 Hz) for each accelerometer is computed for different values of reference temperature ranging from -15 to +45 °C by step of .25 °C (240 samples). For each of these samples, noise is added to the measurements in the following form:

$$a_i(t) = a_i(t) + [\beta \max(a_i(t))] \mathcal{N}(0, 1)(t) \quad (60)$$

where  $a_i(t)$  is the acceleration measured at sensor  $i$ ,  $\mathcal{N}(0, 1)(t)$  is a random Gaussian variable with zero-mean and unitary standard deviation and  $\beta$  is the noise amplitude. For the simulations, different levels of noise were added to the measurements :  $\beta = 0, 0.05, 0.1$  and  $0.2$ . The same computations are repeated after the structure has been damaged (samples 241-480). We consider here four damage scenarios  $d1 - d4$  described in Table 1, the locations  $DL1$ ,  $DL2$  and  $DL3$  are as shown on Fig 7. The different levels of noise are added to the four damage scenarios, so that overall 20 scenarios of 240 samples are computed (5 states : undamaged,  $d1 - d4$ , and 4 noise levels).

damage case	DL1	DL2	DL3
$d1$	1.25 %	3.75 %	2.5 %
$d2$	2.5 %	7.5 %	5 %
$d3$	5 %	15 %	10 %
$d4$	10 %	30 %	20 %

Table 1

Stiffness reduction at locations  $DL1, DL2, DL3$  for the four damage scenarios considered

### 5.3 Feature extraction, factor analysis and statistical process control

Each set of data studied is made of the undamaged state and one of the damaged states. The noise level is the same for the undamaged and the damaged state. The set is made of 480 samples of output-only time responses on the 29 accelerometers situated at the nodes of the finite element model that have a nonzero displacement (Fig 7). Two kinds of feature extraction are performed as explained in section 2: automatic output-only modal analysis using stochastic subspace identification (10 eigenfrequencies and mode shapes for each case), and extraction of peak indicators from the output of the first 9 modal filters. In this second case, a total of 61 features are extracted from the measurements (taking into account the merging of closely spaced eigenfrequencies 3 and 4, and 7 and 8).

The features are then processed in the following manner :

1. A principal component analysis is performed and the first principal components which describe 99.9 % of the variation in the data are kept.
2. Samples 1 through 160 are assumed to be in control, and  $T^2$  is computed using equation (58) and the principal components retained in step 1. A subgroup size of 4 is used which results in a reduction of the number of samples from 480 to 120 (60 undamaged and 60 damaged).
3. The upper control limit is computed using equation (59), with  $\gamma = .999$  and the Shewhart-T control chart is plotted.
4. Factor analysis is performed using 1 out of 2 samples ([1:2:240]) from the undamaged structure, which spans the whole temperature range without including all the samples.
5. Steps 1-3 are repeated for the data after factor analysis.

In Figures 9 through 12, the control charts are presented for damage case  $d4$  and noise level  $\beta = 0$ . The following features are considered:

- the first 10 eigenfrequencies identified using automatic stochastic subspace identification : 10 features.
- mode shapes 1 through 5 extracted using automatic stochastic subspace identification. The mode shapes are normalized with respect to the output of the first accelerometer (out of 29), which results in 28 features for each mode shape : 140 features.
- mode shapes 6 through 10 extracted using automatic stochastic subspace identification. The mode shapes are normalized with respect to the output of the first accelerometer (out of 29), which results in 28 features for each mode shape : 140 features.
- Peak indicators extracted from the output of modal filters : 61 features.

$T^2$  is represented for both the undamaged and the damaged case  $d4$  as a function of the temperature (from  $-15\text{ }^\circ\text{C}$  to  $45\text{ }^\circ\text{C}$ ), together with the upper control limit.

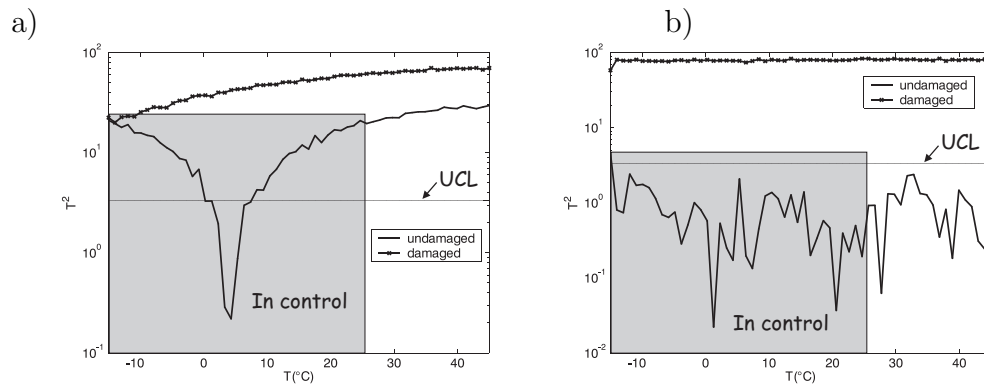


Fig. 9. Shewhart-T control chart for the 10 first eigenfrequencies extracted using stochastic subspace identification a) Raw data, b) After removal of environmental effects (factor analysis)

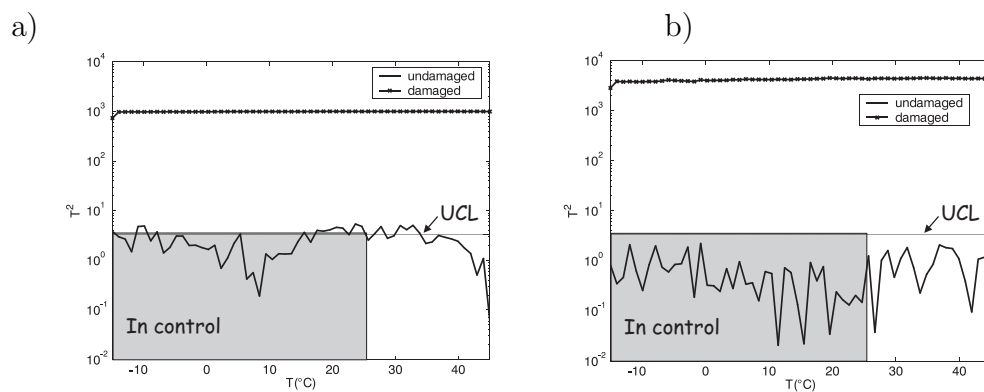


Fig. 10. Shewhart-T control chart for mode shapes 1-5 extracted using stochastic subspace identification a) Raw data, b) After removal of environmental effects (factor analysis)

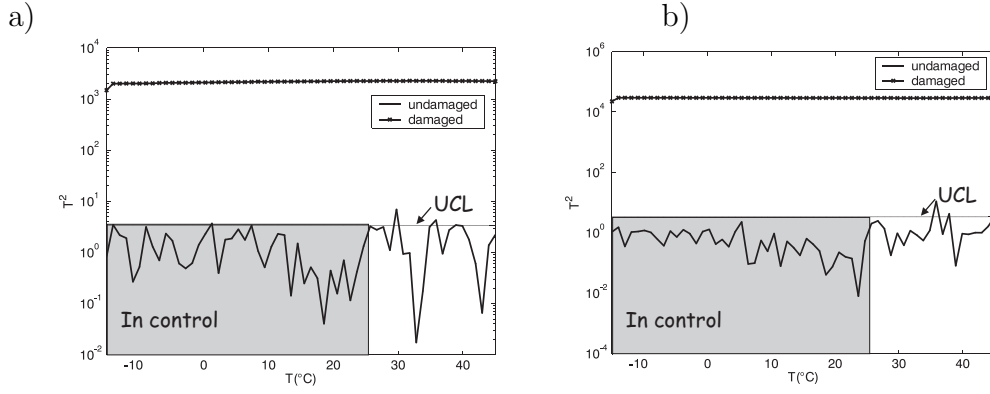


Fig. 11. Shewhart-T control chart for mode shapes 6-10 extracted using stochastic subspace identification a) Raw data, b) After removal of environmental effects (factor analysis)

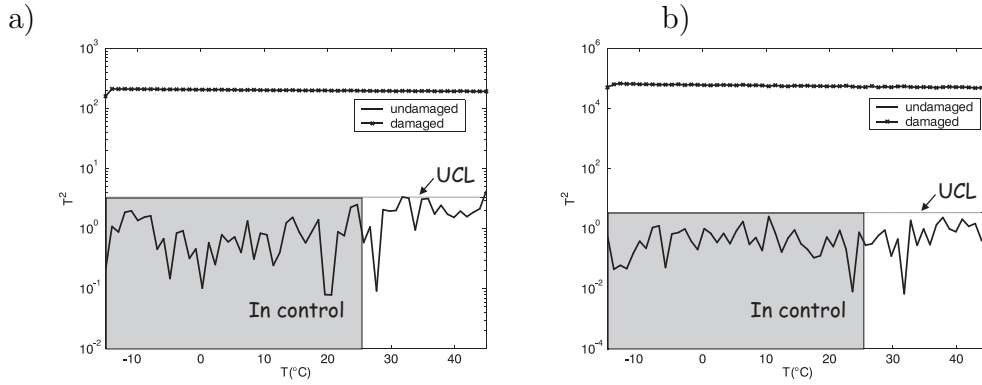


Fig. 12. Shewhart-T control chart for the 61 features extracted from modal filters. a) Raw data, b) After removal of environmental effects (factor analysis)

The figures show that :

- (i) The effects of environment are very pronounced on the eigenfrequencies for which it is impossible to differentiate the damaged state from the undamaged state.
- (ii) This effect is much smaller when using mode shapes. For the control limits however, the F-distribution does not seem to be very well suited, since although the damaged state can be differentiated from the undamaged state,

false alarms arise even for the in control data.

- (iii) For the peak indicators extracted from modal filters, the effect of environment is also very small, and there are false alarms only for the data which is not in control. From that point of view, this indicator seems to be superior to all the others if nothing is done in order to remove the effects of environment.
- (iv) In all cases, factor analysis is efficient in order to remove the effects of environment. A few false alarms still arise for the case of mode shapes 6-10.
- (v) Sensitivity of damage after factor analysis can be compared using the statistics value at damaged state: Frequencies (10 features) 80; mode shapes 1-5 (140 features) 4000; mode shapes 6-10 (140 features) 30 000; peaks from modal filters (61 features) 50 000. High frequency mode shapes are therefore better suited for damage detection than eigenfrequencies, and features extracted from modal features are even more sensitive than all of the other features compared in this paper.

On Fig 13, we study the effect of noise (added in the form of (60) ) on the damage detection for damage case  $d4$ . For clarity, only the damaged case is shown, the undamaged case always lies below the control limit which is the same for all levels of noise, and removal of the environmental effects has been performed.



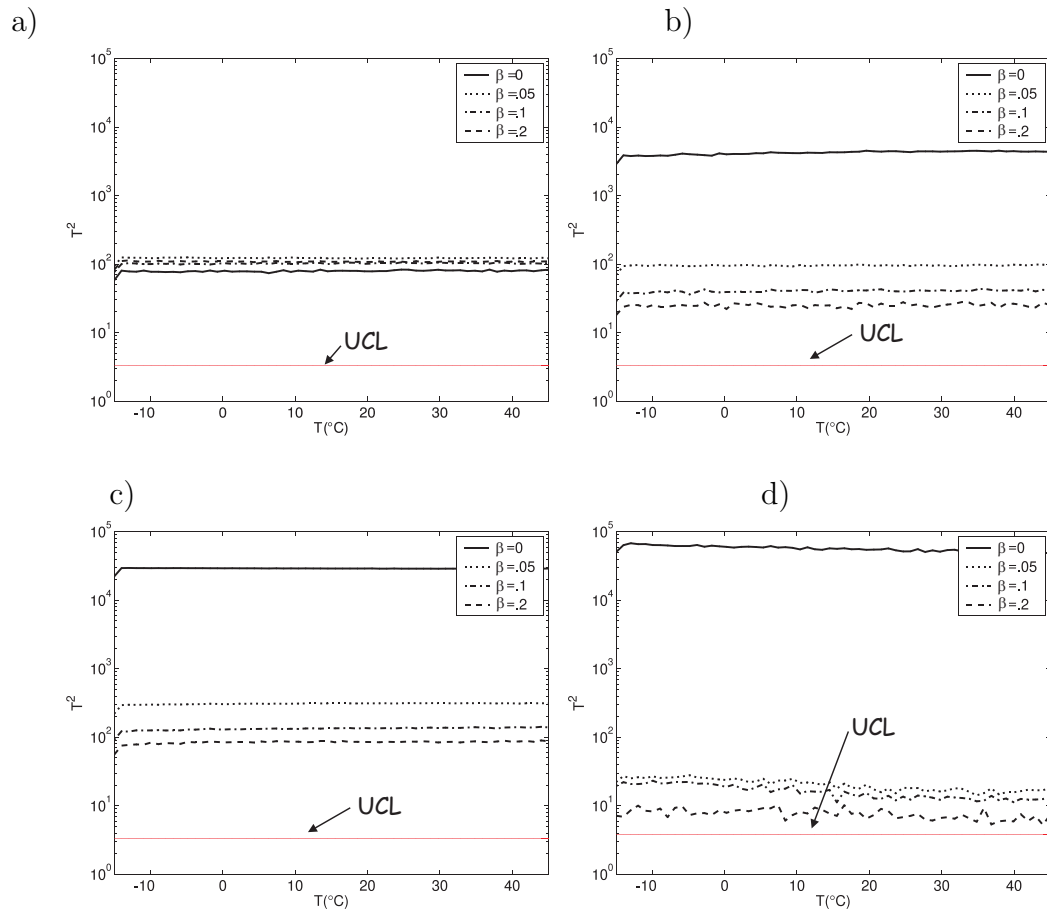


Fig. 13. Shewhart-T control chart for damage case  $d4$  effect of noise on a) 10 first eigenfrequencies, b) mode shapes 1-5, c) mode shapes 6-10, d) features extracted from modal filters

The figures show that :

- (i) the frequencies have a very small sensitivity to noise, the damage detection is not affected by the noise level (even for  $\beta = 0.2$ ).
- (ii) Modeshapes have a high sensitivity to noise, the sensitivity to damage is reduced due to the addition of noise.
- (iii) Modal filter features have a very high sensitivity to noise, the sensitivity to damage is greatly reduced by the presence of noise.

This is further illustrated on Fig 14 where we plot for each noise level a comparison of the value of  $T^2$  for the four different types of features considered. When no noise is added, the features extracted from modal filters are superior to the others, but the performance is degrading fast with the level of noise. For a level of noise of  $\beta = 0.20$ , the best features are the frequencies, which are the worst features when no noise is added. Modeshapes 6-10 present a good compromise, as they are more sensitive than frequencies for low levels of noise, but still comparable for high levels of noise.

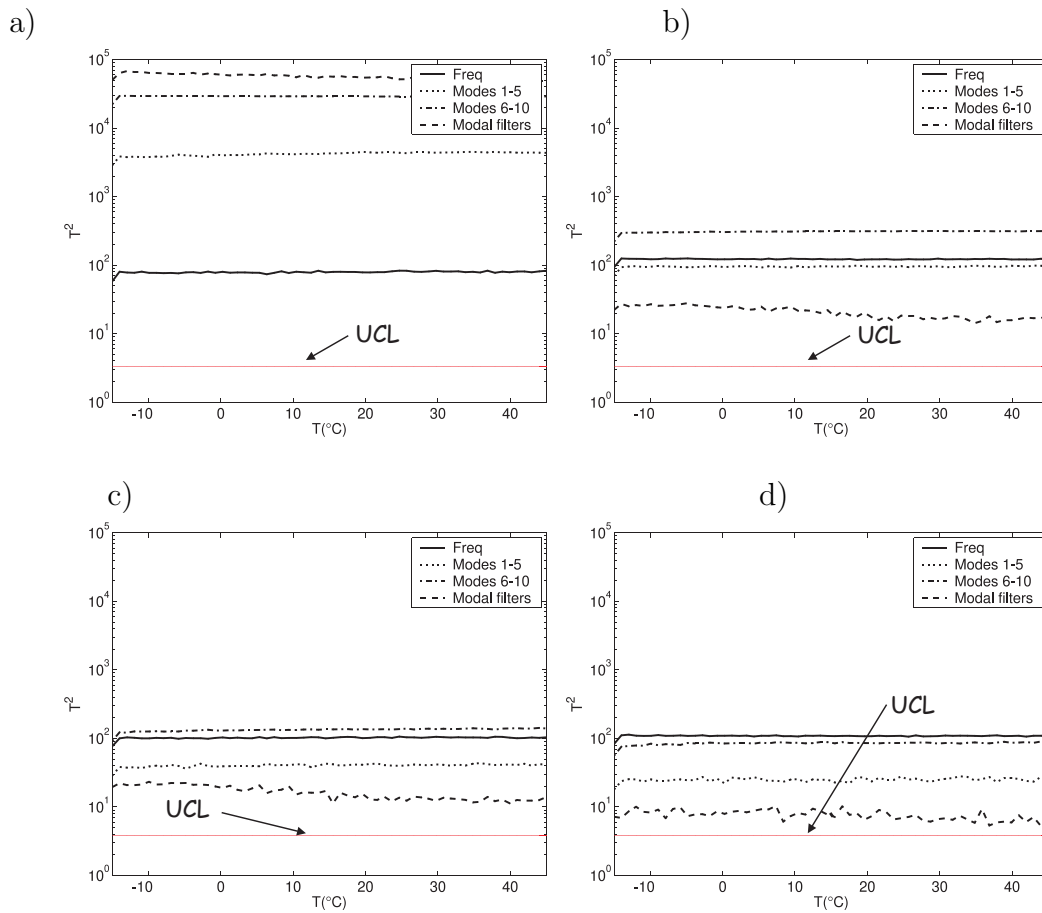


Fig. 14. Shewhart-T control chart for damage case  $d4$  : comparison of the different features for increasing level of noise: a)  $\beta = 0$ , b)  $\beta = 0.05$ , c)  $\beta = 0.10$ , d)  $\beta = 0.20$

On Fig 15, we represent the control charts for each of the features for the

different damage scenarios and  $\beta = 0.05$ . All four types of features have a good behavior (the damage indicator increases with the level of damage), but mode shapes 6-10 are clearly the best indicator for this noise level. Modal filters perform quite poorly due to the presence of a rather small amount of noise.

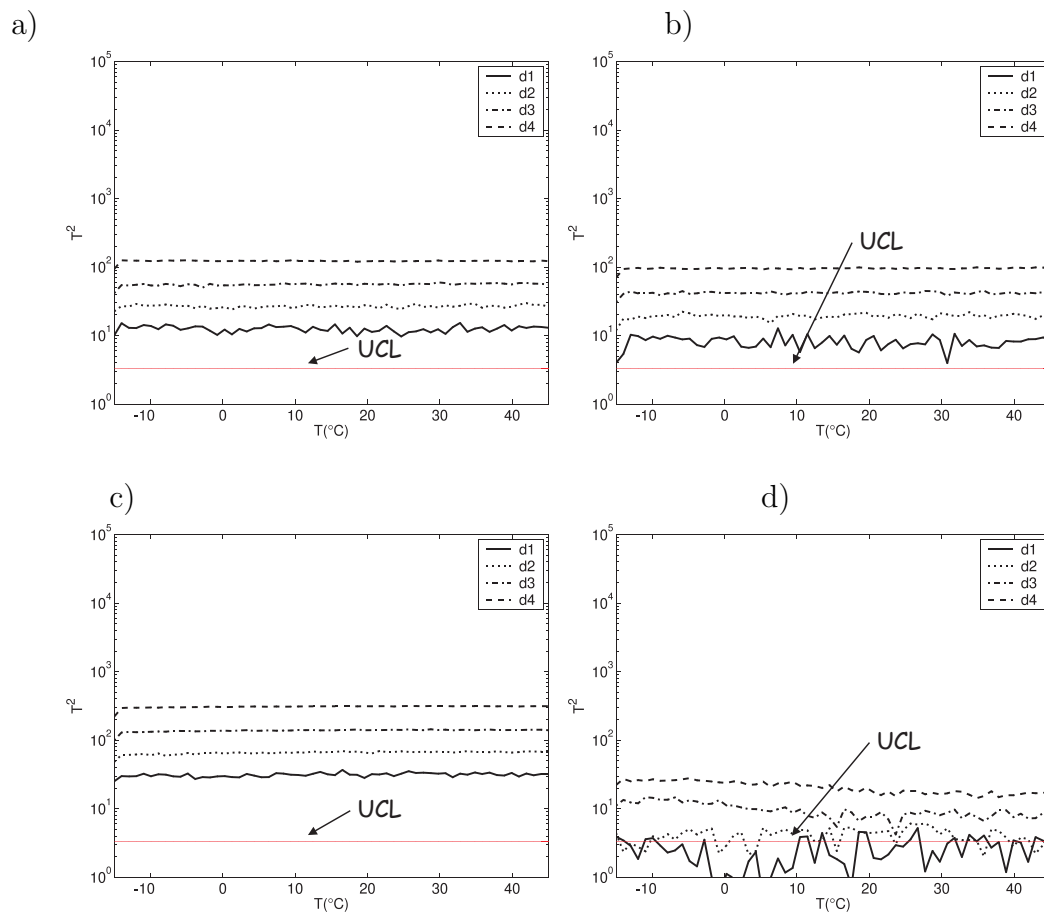


Fig. 15. Shewhart-T control charts for a noise level of  $\beta = 0.05$ , evolution of the damage indicator with the level of damage using the following features a) 10 first eigenfrequencies, b) mode shapes 1-5, c) mode shapes 6-10, d) features extracted from modal filters

#### 5.4 Estimation of computational time

The computations have been run on a PC pentium 4 3.2 Ghz in Matlab under linux environment. Table 2 gives the average computational time for the extraction of features based on the 29 acceleration responses (one set of simulated measurements). Of course efforts could be made to improve the efficiency of the computations for both techniques of feature extraction, this is only an estimation of the initial algorithms. One interesting thing is that both techniques are able to do the extraction of the features in a time smaller than the acquisition time (here 100 s), which means that the features can be estimated in real time in both cases.

Features	Modal filters	Modal data
Computational time (sec)	0.825	40

Table 2

Mean computational time for the extraction of features for one sample of data, using a P4, 3.2 Ghz running linux

Other issues need to be addressed if the methods have to be implemented on a some kind of 'onboard' hardware, such as the memory needed for the computations and the effect of lowering the speed of the processor. These issues are not addressed in the present paper.

#### 5.5 Summary

On table 3, we summarize the advantages and drawbacks of the different features considered in this paper. This table helps to assess which features

should be used depending on the situation (fast computation needed, high level of noise, low level of damage, ....)

Sensitivity to	Freq	Modes 1-5	Modes 6-10	Modal filters
Environment	++	--	--	--
Noise	--	+	+	++
Damage	-	+	++	++
Comp time	-	-	-	--

Table 3

Summary of the sensitivity of the different features to environment, noise, damage, and the associated computational time (-- very low, - low, + high, ++ very high)

## 6 Conclusions

In this paper, we have studied the problem of output-only vibration based damage detection under changing environmental conditions. Two types of features extracted from ambient vibration data have been analyzed : (i) the widely used eigenfrequencies and mode shapes which have been identified using an automated subspace identification procedure and (ii) peak indicators extracted from the output of modal filters. In order to detect damage, statistical process control using Shewhart-T multivariate control chart and principal component analysis have been used. In a last step, based on long term monitoring of the undamaged structure, a statistical model of the effect of environment has been built using factor analysis. This model allows post-processing of the features extracted from the ambient vibration data in order to remove the effect of

environment.

The methodology has been applied to a numerical model of a bridge simulated in the time domain. The bridge is made of different materials whose properties have different variations with respect to temperature. It is subjected to a wide range of temperature gradients, and also to different levels of damage. The numerical results have shown that if nothing is done in order to remove the effects of environment, eigenfrequencies cannot be used in order to detect damage, whereas mode shapes and peaks from modal filters could be used. On the other hand, if factor analysis is used to remove the effects of environment, all the features considered are able to differentiate between the damaged and the undamaged case. When no noise is present in the measurement, the features can be ranked in terms of increasing sensitivity: the least sensitive features are the eigenfrequencies, followed by the low frequency mode shapes, the higher frequency mode shapes and the features extracted from modal filters (most sensitive). When noise is added however, the ranking is different. Frequencies have a very low sensitivity to noise while mode shapes have a much higher sensitivity. The present procedure to compute peak indicators is extremely sensitive to noise, so that even for a relatively low level of noise, the damage detection is strongly affected, and these features are the least sensitive to damage. In the example studied, all the features can be extracted in real time and in an automated way (the time to extract the features is smaller than the length of the acquired signals), which makes them suitable for an automated real-time SHM system.

For average levels of noise, it seems that mode shapes are the ideal candi-

date for output-only SHM under changing environmental conditions. For real structures with very large arrays of sensors (hundreds, thousands ...), it may be that the time needed for the identification becomes prohibitively high. Data reduction is therefore necessary in order to perform the identification in real time. Spatial filters could be used for this purpose. This will be the subject of a future research. An alternative to performing the identification is to use the method of stochastic subspace damage detection described in [37] for which a procedure to treat the environmental effects has also been proposed. A comparison of this method with the procedure presented in this paper is the subject of ongoing research. Finally, experimental investigations are developed in the framework of the ESF Eurocores S3HM project (<http://www.s3hm.be>) in order to validate the present results on real measurements. A small scale mock-up of a cable-stayed bridge has been built and instrumented for that purpose.

## 7 Acknowledgments

This study has been supported by the Belgian Scientific Policy (SSTC return grant, IUAP V - AMS Project), and the FNRS-FRFC . The first author wishes to thank A.M. Yan from the University of Liège for providing the finite element model of the bridge. The research of the fourth author was performed in a MASINA technology program of the Finnish Funding Agency for Technology and Innovation (TEKES). All the authors are partners in the S3HM project (<http://www.s3hm.be>) under the coordination of the ESF Eurocores S3T program.

## References

- [1] O. Salawu, Detection of structural damage through changes in frequency : a review, *Engineering Structures* 19 (9) (1997) 718–723.
- [2] S. Doebling, C. Farrar, M. Prime, A summary review of vibration-based damage identification methods, *Shock and Vibration Digest* 30 (2) (1998) 91–105.
- [3] A. Alvandi, C. Cremona, Assessment of vibration-based damage identification techniques, *Journal of Sound and Vibration* 292 (2006) 179–202.
- [4] D. Montalvao, N. Maia, A. Ribeiro, A review of vibration-based structural health monitoring with special emphasis on composite materials, *Shock and Vibration Digest* 38 (4) (2006) 295–324.
- [5] B. Peeters, G. D. Roeck, Reference-based stochastic subspace identification for output-only modal analysis, *Mechanical Systems and Signal processing* 13(6) (1999) 855–878.
- [6] A. Boukerche, I. Chatzigiannakis, S. Nikolettseas, A new energy efficient and fault-tolerant protocol for data propagation in smart dust networks using varying transmission range, *Computer Communications* 29 (2006) 477–489.
- [7] A. Agogino, I. Tumer, Integrated systems health monitoring using smart dust mote sensor network, in: *Final Report to NASA AMES, 2006, 2006*.
- [8] H. Sohn, M. Dzwonczyk, E. Straser, A. Kiremidjian, K. Law, T. Meng, An experimental study of temperature effect on modal parameters of the alamosa canyon bridge, *Earthquake Engineering and Structural Dynamics* 28 (1999) 878–897.
- [9] S. Alampalli, Effects of testing, analysis, damage and environment on modal parameters, *Mechanical Systems and Signal Processing* 14(1) (2000) 63–74.



- [10] B. Peeters, J. Maeck, G. D. Roeck, Vibration-based damage detection in civil engineering: excitation sources and temperature effects, *Smart materials and Structures* 10 (2001) 518–527.
- [11] B. Peeters, G. D. Roeck, One-year monitoring of the z24-bridge : environmental effects versus damage events, *Earthquake Engineering and Structural Dynamics* 30 (2001) 149–171.
- [12] A. Preumont, A. François, P. D. Man, V. Piefort, Spatial filters in structural control, *Journal of Sound and Vibration* 265 (2003) 61–79.
- [13] A. Deraemaeker, A. Preumont, Vibration based damage detection using large array sensors and spatial filters, *Mechanical Systems and Signal Processing* 20 (2006) 1615–1630.
- [14] Y. Ni, X. Hua, K. Fan, J. Ko, Correlating modal properties with temperature using long-term monitoring data and support vector machine technique, *Engineering Structures* 27 (2005) 1762–1773.
- [15] H. Sohn, M. Dzwonczyk, E. Straser, K. Law, T. Meng, A. Kiremidjian, Adaptive modeling of environmental effects in modal parameters for damage detection in civil structures, in: *Proceedings of SPIE*, 3325, 1998, pp. 127–138.
- [16] J. Kullaa, Structural health monitoring under variable environmental or operational conditions, in: *Proc. of the second European Workshop on Structural Health Monitoring*, Munich, Germany, 2004, pp. 1262–1269.
- [17] G. Manson, Identifying damage sensitive, environment insensitive features for damage detection, in: *Proceedings of the Third International Conference on Identification in Engineering Systems*, 2002.
- [18] A. Yan, G. Kerschen, P. D. Boe, J. Golinval, Structural damaged diagnosis under varying environmental conditions - Part I : A linear analysis, *Mechanical Systems and Signal Processing* 19(4) (2005) 847–864.

- [19] S. Vanlanduit, E. Parloo, B. Cauberghe, P. Guillaume, P. Verboven, A robust singular value decomposition for damage detection under changing operating conditions and structural uncertainties, *Journal of Sound and Vibration* 284 (2005) 1033–1050.
- [20] P. van Overschee, B. D. Moor, *Subspace identification for linear systems*, Kluwer Academic Publishers, Dordrecht, 1996.
- [21] B. Peeters, G. D. Roeck, Reference-based stochastic subspace identification in civil engineering, *Inverse Problems in Engineering* 8 (2000) 47–74.
- [22] E. Reynders, G. De Roeck, Reference-based combined deterministic-stochastic subspace identification for experimental and operational modal analysis, *Mechanical Systems and Signal Processing*, submitted for publication.
- [23] A. Deraemaeker, A. Preumont, J. Kullaa, Modeling and removal of environmental effects for vibration based SHM using spatial filtering and factor analysis, in: *Proc. IMAC XXIV, S.E.M., St Louis, USA, 2006*.
- [24] S. Shelley, L. Freudinger, R. Allemang, Development of an on-line parameter estimation system using the discrete modal filter, in: *S.E.M. (Ed.), Proceedings IMAC X, San Diego, California, 1992*.
- [25] W. Gawronski, Modal actuators and sensors, *Journal of Sound and Vibrations* 229 (4) (2000) 1013–1022.
- [26] K. Jarman, D. Daly, K. Anderson, K. Wahl, A new approach to automated peak detection, *Chemometrics and intelligent laboratory systems* 69 (2003) 61–76.
- [27] R. Danielsson, D. Bylund, K. Markides, Matched filtering with background suppression for improved quality of base peak chromatograms and mass spectra in liquid chromatography-mass spectrometry, *Analytica Chimica Acta* 454 (2002) 167–184.

- [28] I. Daubechies, Ten Lectures on Wavelets, SIAM, 1992.
- [29] G. Manson, B. Lee, W. Staszewski, Eliminating environmental effects from lamb wave-based structural health monitoring, in: Proceedings of ISMA 2004, Leuven, Belgium, 2004, p. 484.
- [30] S. Sharma, Applied multivariate techniques, John Wiley & Sons, New York, 1996.
- [31] J. Kullaa, Structural health monitoring of a crane in variable configurations, in: Proceedings of ISMA 2004, Leuven, Belgium, 2004, pp. 457–469.
- [32] A. Tarantola, Inverse Problem Theory, Elsevier, Amsterdam, 1987.
- [33] D. Montgomery, Introduction to statistical quality control, 3rd Edition, John Wiley & Sons, New York, 1997.
- [34] J. Kullaa, Damage detection of the Z24 bridge using control charts, Mechanical Systems and Signal Processing 17 (1) (2003) 163–170.
- [35] SDTools, Structural dynamics toolbox, <http://www.sdtools.com/>.
- [36] A. Preumont, Frequency domain analysis of time integration operators, Earthquake Engineering and Structural Dynamics 10 (1982) 691–697.
- [37] M. Basseville, M. Abdelghani, A. Benveniste, Subspace-based fault detection algorithms for vibration monitoring, Automatica 36(1) (2000) 101–109.